

Momentum space quantum Monte Carlo on twisted bilayer Graphene

Xu Zhang,^{1,*} Gaopei Pan,^{2,3,*} Yi Zhang,⁴ Jian Kang,⁵ and Zi Yang Meng^{1,2,†}

¹*Department of Physics and HKU-UCAS Joint Institute of Theoretical and Computational Physics,
The University of Hong Kong, Pokfulam Road, Hong Kong SAR, China*

²*Beijing National Laboratory for Condensed Matter Physics and Institute of Physics,
Chinese Academy of Sciences, Beijing 100190, China*

³*School of Physical Sciences, University of Chinese Academy of Sciences, Beijing 100190, China*

⁴*Kavli Institute for Theoretical Sciences, University of Chinese Academy of Sciences, Beijing, 100190, China*

⁵*School of Physical Science and Technology and Institute for Advanced Study, Soochow University, Suzhou, 215006, China*

(Dated: March 7, 2022)

We report an implementation of the momentum space quantum Monte Carlo (QMC) method on the interaction model for the twisted bilayer graphene (TBG). The long-range Coulomb repulsion is treated exactly with the flat bands, spin and valley degrees of freedom of electrons taking into account. We prove the absence of the minus sign problem for QMC simulation when either the two valley or the two spin degrees of freedom are considered. By taking the realistic parameters of the twist angle and interlayer tunnelings into the simulation, we benchmark the QMC data with the exact band gap obtained at the chiral limit, to reveal the insulating ground states at the charge neutrality point (CNP). Then, with the exact Green's functions from QMC, we perform stochastic analytic continuation to obtain the first set of single-particle spectral function for the TBG model at CNP. Our momentum space QMC scheme therefore offers the controlled computation pathway for systematic investigation of the electronic states in realistic TBG model at various electron fillings.

Introduction— Twisted bilayer graphene (TBG) and other moiré systems have attracted great theoretical [1–6] and experimental [7–20] interests in the condensed matter and 2D quantum material communities. As experiments have discovered the correlated insulating phases at various integer fillings and the proximate superconductivity (SC) phases, a key question arises is how to model and understand the properties of the insulating phases, both for their own sake and that could eventually provide a clue for the understanding of the mechanism of the superconductivity in TBG systems.

Many experimental and theoretical works have indicated the interplay between the nontrivial topology and strong interaction as the essential ingredients for the understanding of the electronic correlations in such materials, therefore pointing out a proper model for TBG system shall be significantly different from the typical Hubbard-type Hamiltonian with on-site interactions [21–29]. However, the nature of the insulating states discovered in the material is still under debate. On the one hand, the analytical and the Hartree-Fock calculations at various integer fillings have found the quantum anomalous hall (QAH) and the intervalley coherent (IVC) states as the ground states without breaking the translation symmetry, suggesting that the physics is similar to the quantum Hall ferromagnetism at the lowest Landau level (LLL) [30–40]. Such similarity also led to the proposal of the skyrmion SC for the mechanism of SC discovered near the insulating phases at $\nu = \pm 2$ [41, 42]. On the other hand, recent numerical calculations based on the density matrix renormalization group (DMRG) [41, 43–45]

and exact diagonalization (ED) [46–49] have discovered a larger manifold of nearly degenerate states strongly competing with each other even in the strong coupling regime, hinting that such systems could contain much more complicated physics than that of the LLL. As a consequence, there is a crying need for applying more extensive numerical methodology that can unbiasedly solve larger system sizes to fully settle the mechanism of the insulating phases at various integer fillings.

But this is by no means an easy task. In TBG each moiré superlattice unit cell contains more than 10^4 carbon atoms (in the case close to the first magic angle), resulting in the same number of bands in the moiré Brillouin zone (mBZ). It is impossible to include such a huge number of bands in any realistic calculations for strongly correlated electrons. Fortunately, all experiments have found that the correlated physics emerges only when the chemical potential lies inside the flat bands [7–9] and the large band gap that separates the flat bands and remote bands allows one to focus on the flat bands only to study the electronic correlations [13]. While the parameters of the Hamiltonian has been changed by integrating out the states on the remote bands in the presence of the Coulomb interactions, the effective Hamiltonian is still given by the Bistritzer-MacDonald (BM) model in momentum space [50] with the projected Coulomb interactions onto the flat bands, that has been significantly simplified (yet still difficult) for realistic analytical and numerical calculations [31, 36, 43, 46, 51–56].

In light of the situation, the large-scale quantum Monte Carlo (QMC) method presents itself as the ideal choice of method to solve these TBG models at integer fillings. QMC solves the correlated electron lattice models in path-integral such that both static and dynamic properties, at finite temperature and ground state, can

* These two authors contributed equally

† zymeng@hku.hk

be obtained in unbiased manner with only statistical errors. The extrapolation to the thermodynamic limit is also possible, when the computation complexity increases polynomially with the system sizes, i.e. absence of minus sign problem. Many important features of correlated electron system such as the antiferromagnetic Mott insulator in square lattice Hubbard model [57], non-Fermi liquid at quantum critical points [58, 59], to name a few, have been discovered from QMC simulations. In case of TBG, by now there have been few QMC simulations in real-space lattice model with extended interactions where interaction-driven topological state, IVC and translational symmetry-breaking insulators are found [60–64]. But generic and systematic QMC analysis for BM-type models with flat bands, spin and valley degrees of freedom and in particular, the long-range Coulomb interaction to be fully respected in momentum space, is still missing.

This is the knowledge gap we want to fill in. In this work, we develop a momentum space QMC method [59, 65–67] for the aforementioned TBG models. We first prove the absence of the minus sign problem for QMC simulation at integer fillings when either the two valley or the two spin degrees of freedom are considered. Then, by taking the realistic parameters of the twist angle and interlayer tunnelings into account, we benchmark the QMC data with the exact band gap obtained with a 6×6 momentum mesh in the mBZ, to reveal the insulating ground states at the charge neutrality point (CNP). Finally, by combining the QMC simulation with the stochastic analytic continuation, we obtain the first set of single-particle spectra at chiral limit and realistic parameter at CNP. Our momentum space QMC scheme therefore offers the controlled computation pathway for systematic investigation of the electronic states in realistic TBG model at various electron fillings.

Continuum model— We start from the BM model [1–6] in plane wave basis: $H_{BM}^\tau(\mathbf{k}) = \sum_{\mathbf{k}'} H_{BM\mathbf{k},\mathbf{k}'}^\tau e^{-i\mathbf{k} \cdot \mathbf{r}} e^{i\mathbf{k}' \cdot \mathbf{r}}$ where $H_{BM\mathbf{k},\mathbf{k}'}^\tau = \delta_{\mathbf{k},\mathbf{k}'} \begin{pmatrix} -\hbar v_F(\mathbf{k} - \mathbf{K}_1^\tau) \cdot \boldsymbol{\sigma}^\tau & U_0 \\ U_0^\dagger & -\hbar v_F(\mathbf{k} - \mathbf{K}_2^\tau) \cdot \boldsymbol{\sigma}^\tau \end{pmatrix} + \begin{pmatrix} 0 & U_1^\tau \delta_{\mathbf{k},\mathbf{k}'+\tau\mathbf{G}_1} \\ U_1^{\tau\dagger} \delta_{\mathbf{k},\mathbf{k}'-\tau\mathbf{G}_1} & 0 \end{pmatrix} + \begin{pmatrix} 0 & U_2^\tau \delta_{\mathbf{k},\mathbf{k}'+\tau(\mathbf{G}_1+\mathbf{G}_2)} \\ U_2^{\tau\dagger} \delta_{\mathbf{k},\mathbf{k}'-\tau(\mathbf{G}_1+\mathbf{G}_2)} & 0 \end{pmatrix}$, with $\tau = \pm$ the valley index, $\boldsymbol{\sigma}^\tau = (\tau\sigma_x, \tau\sigma_y)$ defines the A,B sublattices of the monolayer graphene. \mathbf{K}_1^τ and \mathbf{K}_2^τ are the corresponding Dirac points of the bottom and top layers of graphene that are now twisted by angles $\mp \frac{\theta}{2}$,

and $\mathbf{k} \in \text{mBZ}$ and \mathbf{G}_1 and \mathbf{G}_2 are the reciprocal vectors of mBZ, as shown in Fig. 1 (a). The interlayer tunneling between the Dirac states is described by the matrix $U_0 = \begin{pmatrix} u_0 & u_1 \\ u_1 & u_0 \end{pmatrix}$, $U_1^\tau = \begin{pmatrix} u_0 & u_1 e^{-\tau \frac{2\pi i}{3}} \\ u_1 e^{\tau \frac{2\pi i}{3}} & u_0 \end{pmatrix}$ and $U_2^\tau = \begin{pmatrix} u_0 & u_1 e^{\tau \frac{2\pi i}{3}} \\ u_1 e^{-\tau \frac{2\pi i}{3}} & u_0 \end{pmatrix}$ where u_0 and u_1 are the intra-sublattice and inter-sublattice interlayer tunneling amplitudes. The flatness of the lowest two bands per spin per valley in the chiral limit ($u_0=0$) is determined by the dimensionless parameter $\alpha = \frac{u_1}{\hbar v_F k_\theta}$ with $k_\theta = 8\pi \sin(\theta/2)/(3a_0)$ and the lattice constant of the monolayer graphene $a_0=0.246$ nm. In this paper, we choose $\hbar v_F/a_0=2.37745$ eV, the twist angle $\theta=1.08^\circ$ and $u_1=0.11$ eV which leads to $\alpha=0.586$, the value corresponding to the first magic angle where the lowest two bands become completely flat in the chiral limit. We perform the QMC simulation at both the chiral limit ($u_0 = 0$) and the more realistic case ($u_0 = 0.06$ eV), which leads to a bandwidth of 1.08 meV.

The eigenstate of H_{BM}^τ can be written in the Bloch wavefunction form $\psi_{m,\tau,\mathbf{k}}^X(\mathbf{r}) = \sum_{\mathbf{G}} u_{m,\tau;\mathbf{G},X}(\mathbf{k}) e^{i(\mathbf{k}+\mathbf{G}) \cdot \mathbf{r}}$ where $X = \{A_1, B_1, A_2, B_2\}$ denotes the layer and sublattice indices and $u_{m,\tau;\mathbf{G},X}(\mathbf{k})$ is the Bloch wave-function with the eigen-energy $\epsilon_{m\mathbf{k}\tau}$. Here, m and τ are the band and valley indices and we omit the spin index s for now since the Hamiltonian is spin independent. The range of m can be large (consider the couplings $\{\mathbf{k}, \mathbf{k} + \mathbf{G}_1, \mathbf{k} + \mathbf{G}_1 + \mathbf{G}_2, \dots\}$ in Fig. 1 (a) which has $m \in 1, 2, \dots, M$ elements, then $H_{BM\mathbf{k},\mathbf{k}'}^\tau$ is a $4M \times 4M$ matrix), we select the two flat bands and denote them as $m = 1, 2$ and consider the projected Coulomb interactions onto these bands in this work.

Interaction model and QMC Implementations— We develop a momentum space QMC scheme to solve the interaction Hamiltonian in the band basis:

$$H_{int} = \frac{1}{2\Omega} \sum_{\mathbf{q}, \mathbf{G}, i|\mathbf{q}+\mathbf{G}| \neq 0} V(\mathbf{q} + \mathbf{G}) \delta \rho_{\mathbf{q}+\mathbf{G}} \delta \rho_{-\mathbf{q}-\mathbf{G}}, \quad (1)$$

as shown in Fig. 1 (a), $\mathbf{q} \in \text{mBZ}$ and $\mathbf{q} + \mathbf{G}$ represents a vector in extended mBZ, and we consider the momentum transfer upto the distance of \mathbf{G}_1 and \mathbf{G}_2 [52, 53], as denoted by the yellow dots in the figure. The single gate Coulomb interaction is long-ranged: $V(\mathbf{q}) = \frac{e^2}{4\pi\epsilon} \int d^2\mathbf{r} \left(\frac{1}{r} - \frac{1}{\sqrt{r^2+d^2}} \right) e^{i\mathbf{q} \cdot \mathbf{r}} = \frac{e^2}{2\epsilon} \frac{1}{q} (1 - e^{-qd})$ with $\frac{d}{2}$ is the distance between graphene layer and single gate and ϵ is the dielectric constant.

The definition of $\delta \rho_{\mathbf{q}+\mathbf{G}}$ is:

$$\delta \rho_{\mathbf{q}+\mathbf{G}} = \sum_{\mathbf{k} \in \text{mBZ}, m_1, m_2, \tau, s} \lambda_{m_1, m_2, \tau}(\mathbf{k}, \mathbf{k} + \mathbf{q} + \mathbf{G}) (d_{\mathbf{k}, m_1, \tau, s}^\dagger d_{\mathbf{k}+\mathbf{q}, m_2, \tau, s} - \frac{1}{2} \delta_{\mathbf{q}, 0} \delta_{m_1, m_2}) = (\delta \rho_{-\mathbf{q}-\mathbf{G}})^\dagger \quad (2)$$

with the form factor λ defined as $\lambda_{m_1, m_2, \tau}(\mathbf{k}, \mathbf{k} + \mathbf{q} + \mathbf{G}) =$

$\sum_{\mathbf{G}', X} u_{m_1, \tau; \mathbf{G}', X}^*(\mathbf{k}) u_{m_2, \tau; \mathbf{G}'+\mathbf{G}, X}(\mathbf{k} + \mathbf{q})$. Physically, $\delta \rho$

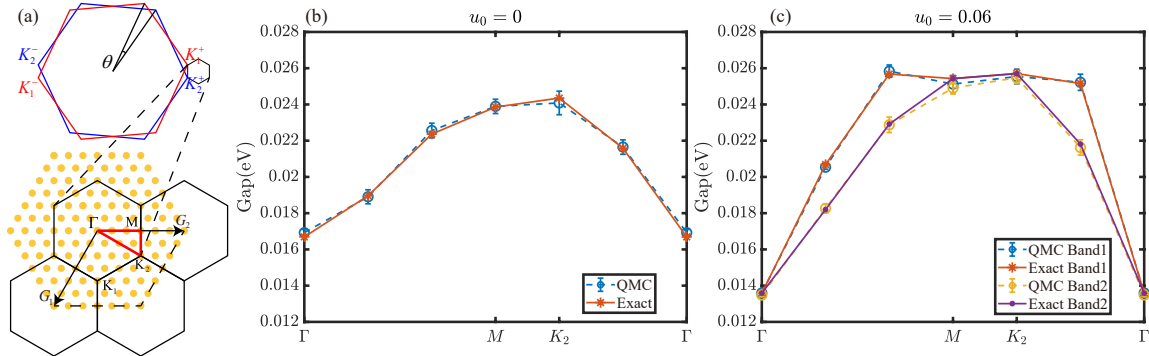


FIG. 1. (a) Upper panel shows the Brillouin zone foldings in TBG, with the small hexagon representing the mBZ. $\mathbf{K}_{1,2}^{\pm}$ are the Dirac points for valley \pm and layer 1 and 2, θ is the rotating angle. In lower panel, \mathbf{G}_1 and \mathbf{G}_2 are the reciprocal lattice vectors of the mBZ. The yellow dots are the allowed momentum transfer \mathbf{q} points in QMC. Here we consider momentum transfer upto \mathbf{G} , which means for a 6×6 mesh in mBZ, the allowed number of \mathbf{q} is 126. (b) and (c) show the comparison at the CNP of the single-particle excitation gap at the chiral limit ($u_0 = 0$ eV) and realistic case ($u_0 = 0.06$ eV) between exact solution and the QMC results. The QMC gaps are obtained from fitting the imaginary time decay of the fermion Green's function.

is the electron density operator relative to the decoupled bilayer graphene at the CNP. The interaction in Eq. (1) differs from the normal ordered version as it can properly account for the renormalization effect of the remote bands to the flat bands [53]. The symmetry properties

of $\lambda_{m_1, m_2, \tau}(\mathbf{k}, \mathbf{k} + \mathbf{q} + \mathbf{G})$ are discussed in Supplemental Material (SM) [68]. One sees $\delta\rho_{\mathbf{q}+\mathbf{G}}$ in single particle basis is a block diagonal matrix according to the τ, s indices. Since $V(\mathbf{q} + \mathbf{G}) = V(-\mathbf{q} - \mathbf{G})$, terms in H_{int} can be written in a form ready to be QMC decoupled as,

$$\sum_{\mathbf{q}, \mathbf{G}, |\mathbf{q}+\mathbf{G}| \neq 0} V(\mathbf{q} + \mathbf{G}) \delta\rho_{\mathbf{q}+\mathbf{G}} \delta\rho_{-\mathbf{q}-\mathbf{G}} = \sum_{|\mathbf{q}+\mathbf{G}| \neq 0} \frac{V(\mathbf{q} + \mathbf{G})}{2} \left[(\delta\rho_{-\mathbf{q}-\mathbf{G}} + \delta\rho_{\mathbf{q}+\mathbf{G}})^2 - (\delta\rho_{-\mathbf{q}-\mathbf{G}} - \delta\rho_{\mathbf{q}+\mathbf{G}})^2 \right] \quad (3)$$

where $\sum_{|\mathbf{q}+\mathbf{G}| \neq 0}$ means summation to half of the allowed values of \mathbf{q} and \mathbf{G} .

According to the discrete Hubbard-Stratonovich transformation [60, 61, 69], $e^{\alpha \hat{O}^2} = \frac{1}{4} \sum_{l=\pm 1, \pm 2} \gamma(l) e^{\sqrt{\alpha} \eta(l) \hat{O}} + O(\alpha^4)$, where $\gamma(\pm 1) = 1 + \frac{\sqrt{6}}{3}$, $\gamma(\pm 2) = 1 - \frac{\sqrt{6}}{3}$, $\eta(\pm 1) = \pm \sqrt{2(3 - \sqrt{6})}$ and $\eta(\pm 2) = \pm \sqrt{2(3 + \sqrt{6})}$, we can rewrite the partition function of Hamiltonian Eq. (1) in the imaginary time discretization as,

$$\begin{aligned} Z &= \text{Tr} \left\{ \prod_t e^{-\Delta\tau H_{int}(t)} \right\} = \text{Tr} \left\{ \prod_t e^{-\Delta\tau \frac{1}{4\Omega} \sum_{|\mathbf{q}+\mathbf{G}| \neq 0} V(\mathbf{q}+\mathbf{G}) [(\delta\rho_{-\mathbf{q}-\mathbf{G}} + \delta\rho_{\mathbf{q}+\mathbf{G}})^2 - (\delta\rho_{-\mathbf{q}-\mathbf{G}} - \delta\rho_{\mathbf{q}+\mathbf{G}})^2]} \right\} \\ &\approx \sum_{\{l_{|\mathbf{q}|,t}\}} \prod_t \left[\prod_{|\mathbf{q}+\mathbf{G}| \neq 0} \frac{1}{16} \gamma(l_{|\mathbf{q}|,t}) \gamma(l_{|\mathbf{q}|,2,t}) \right] \text{Tr} \left\{ \prod_t \left[\prod_{|\mathbf{q}+\mathbf{G}| \neq 0} e^{i\eta(l_{|\mathbf{q}|,t}) A_{\mathbf{q}} (\delta\rho_{-\mathbf{q}} + \delta\rho_{\mathbf{q}})} e^{\eta(l_{|\mathbf{q}|,2,t}) A_{\mathbf{q}} (\delta\rho_{-\mathbf{q}} - \delta\rho_{\mathbf{q}})} \right] \right\} \quad (4) \end{aligned}$$

where t is the imaginary time index with step $\Delta\tau$, $A_{\mathbf{q}+\mathbf{G}} = \sqrt{\frac{\Delta\tau}{4} \frac{V(\mathbf{q}+\mathbf{G})}{\Omega}}$ and $\{l_{|\mathbf{q}|,1,t}, l_{|\mathbf{q}|,2,t}, l_{0,t}\}$ are the four-component auxiliary field that lives in the space-time configuration of the path-integral. For each realization of the auxiliary field configuration, the fermion determinant can be evaluated exactly as the configurational weight, the QMC simulation is performed along a Markov chain of such configurations and the important sampling can be carried out with the physical observables (such as single-particle Green's function) computed through ensemble average [70].

One shall be careful about the approxima-

tion " \approx " in Eq. (4). Since $\delta\rho_{\mathbf{q}+\mathbf{G}} \delta\rho_{\mathbf{q}'+\mathbf{G}'} - \delta\rho_{\mathbf{q}'+\mathbf{G}'} \delta\rho_{\mathbf{q}+\mathbf{G}} = \sum_{\mathbf{k}, m_1, m_2, \tau, s} [\lambda_{\tau}(\mathbf{k}, \mathbf{k} + \mathbf{q} + \mathbf{G}) \lambda_{\tau}(\mathbf{k}, \mathbf{k} + \mathbf{q}' + \mathbf{G}') - \lambda_{\tau}(\mathbf{k}, \mathbf{k} + \mathbf{q}' + \mathbf{G}') \lambda_{\tau}(\mathbf{k}, \mathbf{k} + \mathbf{q} + \mathbf{G})]_{m_1, m_2} d_{\mathbf{k}, m_1, \tau, s}^{\dagger} d_{\mathbf{k}+\mathbf{q}+\mathbf{q}', m_2, \tau, s}$, which means $[\delta\rho_{\mathbf{q}+\mathbf{G}}, \delta\rho_{\mathbf{q}'+\mathbf{G}'}] \neq 0$. However when the number of \mathbf{q} is limited as shown in Fig. 1 (a), i.e. allowing momentum transfer upto \mathbf{G} , our results show the systematic discretization errors are acceptable. By setting $\varepsilon = 7\varepsilon_0$, the moiré lattice vector $L_M = \frac{a_0}{2 \sin(\frac{\theta}{2})}$, the area of system $\Omega = N_{\mathbf{k}} \frac{\sqrt{3}}{2} L_M^2$ with $N_{\mathbf{k}}$ the number of \mathbf{k} points in mBZ (here we have $N_{\mathbf{k}} = 36$ for the 6×6 mesh), and the gate distance

$d = 40$ nm, mBZ reciprocal lattice vector $|\mathbf{G}| = \frac{4\pi}{\sqrt{3}L_M}$, we have $\frac{V(\bar{\mathbf{q}})}{\Omega} \approx 0.01585 \frac{1}{\sqrt{N_k}} \left(1 - e^{-22.36 \frac{1}{\sqrt{N_k}} \bar{\mathbf{q}}}\right)$ eV where $\bar{\mathbf{q}}$ is the distance between momenta in mBZ by setting two nearest \mathbf{k} points with unit length.

Discussion of the sign-problem— We note in Eq. (4), the exponential parts of decoupled interaction are anti-Hermitian, the following three statements about the sign structure of the QMC fermion determinants are in order:

Statement 1 Considering single valley and single spin without kinetic terms at half filling, the sign of the determinant is always real.

Proof In our decoupled Hamiltonian, the configurational probability is proportional to $e^{-\frac{1}{2} \sum_j \text{Tr}(M_j)} \det(I + e^{M_1} e^{M_2} \dots e^{M_n})$. Here M_j are anti-Hermitian matrices in single particle basis and $e^{-\frac{1}{2} \sum_j \text{Tr}(M_j)}$ comes from constant terms in $\delta\rho_{\mathbf{q}+\mathbf{G}}$. Since e^{M_j} are unitary matrices, $U = e^{M_1} e^{M_2} \dots e^{M_n}$ is also unitary with eigenvalue $e^{i\lambda_j}$. Set $\det(U) = e^{\sum_j \text{Tr}(M_j)} = e^{\sum_j i\lambda_j} = e^{i\Gamma}$, $e^{-i\frac{1}{2} \det(I + U)} = e^{-i\frac{1}{2} \prod_j (1 + e^{i\lambda_j})}$. For any term $e^{i(\sum_{k \in A} \lambda_k - \frac{\Gamma}{2})}$, $A \subseteq \{1, 2, \dots, n\}$, there is always a term $e^{i(\sum_{k \notin A} \lambda_k - \frac{\Gamma}{2})} = e^{-i(\sum_{k \in A} \lambda_k - \frac{\Gamma}{2})}$, so add all terms together will always be real.

Statement 2 Considering single valley and double spin without kinetic terms at half filling, there is no sign problem.

Proof It is straightforward to see this result according to Statement 1 by noticing the other spin just gives a copy so that the real sign will become a non-negative sign. But kinetic terms could change this result. See SM [68] for details.

Statement 3 Considering single spin and double valley with flat band kinetic terms at half filling, there is no sign problem.

Proof One can relabel $d_{k,m,-\tau,s}$ as $-m * \tilde{d}_{k,-m,-\tau,s}^\dagger$ in $-\tau$ subspace, then prove the single-particle matrixes between two valleys satisfy $\delta\rho_{\mathbf{q}+\mathbf{G},-\tau} = -\delta\rho_{-\mathbf{q}-\mathbf{G},\tau}$. Thus $M_{j,-\tau} = M_{j,\tau}^*$. And this transformation will keep flat band kinetic matrices intact between two valleys. So the determinant of valley $-\tau$ is complex conjugated with that of valley τ . We note similar observation, that the TBG Hamiltonian at CNP after QMC decoupling is invariant under anti-unitary particle-hole symmetry and thus free of the sign problem, has also been pointed out in Ref. [71].

We organize these statements in Tab. I. And we noted that Ref. [72] also shows some similar results.

TABLE I. List of the sign structure for TBG Hamiltonian.

| Degrees of freedom | Kinetic terms | Sign Structure |
|---------------------------|---------------|----------------|
| Single valley single spin | No | Real |
| Single valley double spin | No | Non-negative |
| Double valley single spin | Flat bands | Non-negative |
| Double valley double spin | Flat bands | Non-negative |

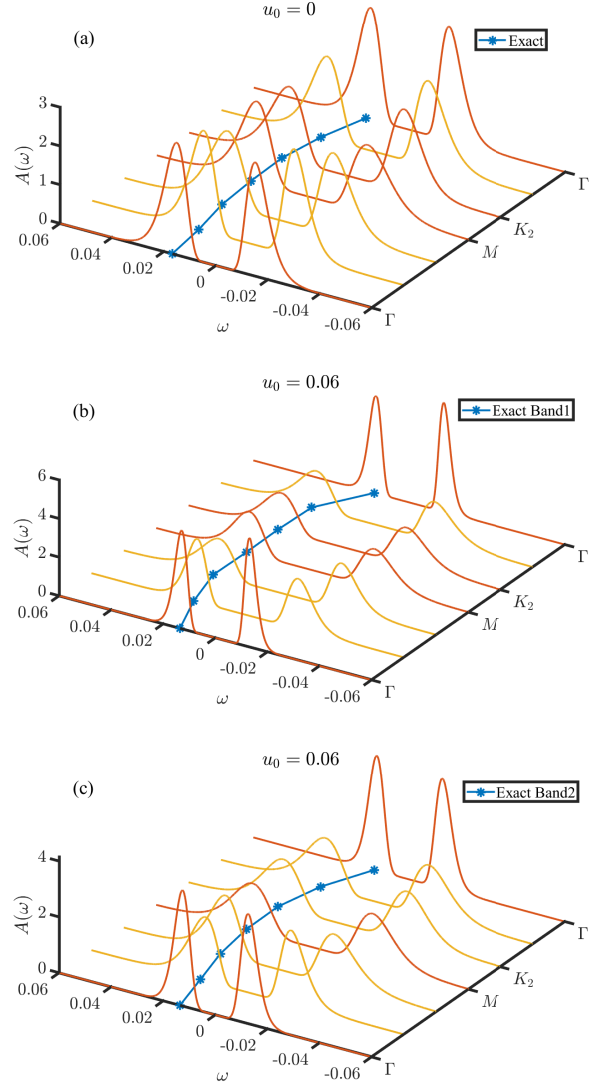


FIG. 2. Single-particle spectra obtained from QMC+SAC at CNP with (a) chiral limit ($u_0 = 0$) and (b), (c) $u_0 = 0.06$. The exact gaps are the same as in Fig. 1 (b) and (c).

QMC Results and Discussions— With such understanding, we carried out QMC simulations at CNP for TBG Hamiltonian in momentum-space, on the grids of 6×6 in mBZ, both at chiral limit ($u_0 = 0$) and with realistic parameter ($u_0 = 0.06$). To make sure our QMC have converged to the ground state, we set the temperature $T = 0.667$ meV in the simulations, which turns out to be magnitudes smaller than the obtained gap, and divide the inverse temperature $\beta = 1/T$ to 150 pieces with $\Delta\tau = 0.01$ such that the Trotter error negligible.

Fig. 1 (b) and (c) show the comparison of the single-particle excitation gap at the chiral limit ($u_0 = 0$) and $u_0 = 0.06$, obtained from fitting the imaginary decay of the Green's function in QMC simulations, respectively. At the chiral limit, the two bands are degenerate, whereas in the realistic case, we diagonalize the Green's function

at every \mathbf{k} point in the 2×2 band basis. The agreement between the exact gaps [55] and the QMC ones is perfect.

Fig. 2 show the single-particle spectra, obtained from applying stochastically analytic continuation (SAC) [73–77] upon the imaginary time Green’s function from QMC simulations. Such QMC+SAC scheme has been shown to reliably reveal many interesting dynamical features in various strongly correlated systems [77–86]. Fig. 2 (a) shows the single-particle spectrum at the chiral limit ($u_0 = 0$) where the two bands are degenerate and Fig. 2 (b) and (c) the spectral of the two bands at $u_0 = 0.06$ where they are not degenerate. In all cases, the spectral are particle-hole symmetric.

With the establishment of such unbiased QMC computational framework, as summarized in Tab. I, the controlled computation pathway for the interaction effects in realistic TBG model is clearly opening up. The questions of the nature of the ground states at different integer fillings and the TBG phase diagram at different twist angle, chiral ratio, hNB alignment, the skyrmion SC and the dynamic and spectral properties, etc, can now be investigated as those have been investigated with QMC

simulations in other exotic strongly correlated electron systems [87–90].

Acknowledgments— ZYM thanks Xi Dai for the insightful discussion and continuous encouragement for addressing the momentum-space solutions of TBG. XZ, GPP and ZYM acknowledge support from the RGC of Hong Kong SAR of China (Grant Nos. 17303019, 17301420 and AoE/P-701/20), MOST through the National Key Research and Development Program (Grant No. 2016YFA0300502) and the Strategic Priority Research Program of the Chinese Academy of Sciences (Grant No. XDB33000000). YZ is supported in part by the strategic priority research program of the Chinese Academy of Sciences Grant No. XDB28000000 and NSFC Grant Nos. 11674278, 12004383 and 12074276 and the Fundamental Research Funds for the Central Universities. JK acknowledges the support from the NSFC Grant No. 12074276, and the Priority Academic Program Development (PAPD) of Jiangsu Higher Education Institutions. We thank the Computational Initiative at the Faculty of Science and the Information Technology Services at the University of Hong Kong for their technical support and generous allocation of CPU time.

-
- [1] G. Trambly de Laissardière, D. Mayou, and L. Magaud, *Nano Letters* **10**, 804 (2010).
 - [2] G. Trambly de Laissardière, D. Mayou, and L. Magaud, *Phys. Rev. B* **86**, 125413 (2012).
 - [3] R. Bistritzer and A. H. MacDonald, *Proceedings of the National Academy of Sciences* **108**, 12233 (2011).
 - [4] A. Rozhkov, A. Sboychakov, A. Rakhmanov, and F. Nori, *Physics Reports* **648**, 1 (2016), electronic properties of graphene-based bilayer systems.
 - [5] J. M. B. Lopes dos Santos, N. M. R. Peres, and A. H. Castro Neto, *Phys. Rev. Lett.* **99**, 256802 (2007).
 - [6] J. M. B. Lopes dos Santos, N. M. R. Peres, and A. H. Castro Neto, *Phys. Rev. B* **86**, 155449 (2012).
 - [7] Y. Cao, V. Fatemi, S. Fang, K. Watanabe, T. Taniguchi, E. Kaxiras, and P. Jarillo-Herrero, *Nature* **556**, 43 (2018).
 - [8] Y. Cao, V. Fatemi, A. Demir, S. Fang, S. L. Tomarken, J. Y. Luo, J. D. Sanchez-Yamagishi, K. Watanabe, T. Taniguchi, E. Kaxiras, *et al.*, *Nature* **556**, 80 (2018).
 - [9] G. Chen, A. L. Sharpe, E. J. Fox, Y.-H. Zhang, S. Wang, L. Jiang, B. Lyu, H. Li, K. Watanabe, T. Taniguchi, *et al.*, *Nature* **579**, 56 (2020).
 - [10] A. Kerelsky, L. J. McGilly, D. M. Kennes, L. Xian, M. Yankowitz, S. Chen, K. Watanabe, T. Taniguchi, J. Hone, C. Dean, *et al.*, *Nature* **572**, 95 (2019).
 - [11] S. L. Tomarken, Y. Cao, A. Demir, K. Watanabe, T. Taniguchi, P. Jarillo-Herrero, and R. C. Ashoori, *Phys. Rev. Lett.* **123**, 046601 (2019).
 - [12] X. Lu, P. Stepanov, W. Yang, M. Xie, M. A. Aamir, I. Das, C. Urgell, K. Watanabe, T. Taniguchi, G. Zhang, *et al.*, *Nature* **574**, 653 (2019).
 - [13] Y. Xie, B. Lian, B. Jäck, X. Liu, C.-L. Chiu, K. Watanabe, T. Taniguchi, B. A. Bernevig, and A. Yazdani, *Nature* **572**, 101 (2019).
 - [14] C. Shen, Y. Chu, Q. Wu, N. Li, S. Wang, Y. Zhao, J. Tang, J. Liu, J. Tian, K. Watanabe, T. Taniguchi, R. Yang, Z. Y. Meng, D. Shi, O. V. Yazyev, and G. Zhang, *Nature Physics* (2020), 10.1038/s41567-020-0825-9.
 - [15] K. P. Nuckolls, M. Oh, D. Wong, B. Lian, K. Watanabe, T. Taniguchi, B. A. Bernevig, and A. Yazdani, *Nature* **588**, 610 (2020).
 - [16] A. T. Pierce, Y. Xie, J. M. Park, E. Khalaf, S. H. Lee, Y. Cao, D. E. Parker, P. R. Forrester, S. Chen, K. Watanabe, T. Taniguchi, A. Vishwanath, P. Jarillo-Herrero, and A. Yacoby, “Unconventional sequence of correlated chern insulators in magic-angle twisted bilayer graphene,” (2021), arXiv:2101.04123 [cond-mat.mes-hall].
 - [17] S. Moriyama, Y. Morita, K. Komatsu, K. Endo, T. Iwasaki, S. Nakaharai, Y. Noguchi, Y. Wakayama, E. Watanabe, D. Tsuya, K. Watanabe, and T. Taniguchi, *arXiv e-prints*, arXiv:1901.09356 (2019), arXiv:1901.09356 [cond-mat.supr-con].
 - [18] A. Rozen, J. M. Park, U. Zondiner, Y. Cao, D. Rodan-Legrain, T. Taniguchi, K. Watanabe, Y. Oreg, A. Stern, E. Berg, *et al.*, *arXiv preprint arXiv:2009.01836* (2020).
 - [19] X. Liu, C.-L. Chiu, J. Y. Lee, G. Farahi, K. Watanabe, T. Taniguchi, A. Vishwanath, and A. Yazdani, *arXiv preprint arXiv:2008.07552* (2020).
 - [20] C. Shen, J. Ying, L. Liu, J. Liu, N. Li, S. Wang, J. Tang, Y. Zhao, Y. Chu, K. Watanabe, T. Taniguchi, R. Yang, D. Shi, F. Qu, L. Lu, W. Yang, and G. Zhang, *Chinese Physics Letters* **38**, 047301 (2021).
 - [21] H. C. Po, H. Watanabe, and A. Vishwanath, *Phys. Rev. Lett.* **121**, 126402 (2018).
 - [22] H. C. Po, L. Zou, T. Senthil, and A. Vishwanath, *Phys. Rev. B* **99**, 195455 (2019).

- [23] N. Bultinck, S. Chatterjee, and M. P. Zaletel, Phys. Rev. Lett. **124**, 166601 (2020).
- [24] H. C. Po, L. Zou, A. Vishwanath, and T. Senthil, Phys. Rev. X **8**, 031089 (2018).
- [25] G. Tarnopolsky, A. J. Kruchkov, and A. Vishwanath, Phys. Rev. Lett. **122**, 106405 (2019).
- [26] N. F. Q. Yuan and L. Fu, Phys. Rev. B **98**, 045103 (2018).
- [27] J. Kang and O. Vafeek, Phys. Rev. X **8**, 031088 (2018).
- [28] M. Koshino, N. F. Q. Yuan, T. Koretsune, M. Ochi, K. Kuroki, and L. Fu, Phys. Rev. X **8**, 031087 (2018).
- [29] B. Roy and V. Jurićić, Phys. Rev. B **99**, 121407 (2019).
- [30] Y. Zhang, K. Jiang, Z. Wang, and F. Zhang, Phys. Rev. B **102**, 035136 (2020).
- [31] N. Bultinck, E. Khalaf, S. Liu, S. Chatterjee, A. Vishwanath, and M. P. Zaletel, Phys. Rev. X **10**, 031034 (2020).
- [32] K. Hejazi, X. Chen, and L. Balents, Phys. Rev. Research **3**, 013242 (2021).
- [33] M. Xie and A. H. MacDonald, Phys. Rev. Lett. **124**, 097601 (2020).
- [34] J. Liu, J. Liu, and X. Dai, Phys. Rev. B **99**, 155415 (2019).
- [35] J. Liu and X. Dai, npj Computational Materials **6**, 1 (2020).
- [36] J. Liu and X. Dai, Phys. Rev. B **103**, 035427 (2021).
- [37] T. Cea and F. Guinea, Phys. Rev. B **102**, 045107 (2020).
- [38] S. Liu, E. Khalaf, J. Y. Lee, and A. Vishwanath, Phys. Rev. Research **3**, 013033 (2021).
- [39] S. Carr, S. Fang, Z. Zhu, and E. Kaxiras, Phys. Rev. Research **1**, 013001 (2019).
- [40] Y. H. Kwan, G. Wagner, T. Soejima, M. P. Zaletel, S. H. Simon, S. A. Parameswaran, and N. Bultinck, arXiv e-prints, arXiv:2105.05857 (2021), arXiv:2105.05857 [cond-mat.str-el].
- [41] S. Chatterjee, M. Ippoliti, and M. P. Zaletel, arXiv e-prints, arXiv:2010.01144 (2020), arXiv:2010.01144 [cond-mat.str-el].
- [42] E. Khalaf, S. Chatterjee, N. Bultinck, M. P. Zaletel, and A. Vishwanath, Science Advances **7** (2021), 10.1126/sciadv.abf5299.
- [43] J. Kang and O. Vafeek, Phys. Rev. B **102**, 035161 (2020).
- [44] T. Soejima, D. E. Parker, N. Bultinck, J. Hauschild, and M. P. Zaletel, Phys. Rev. B **102**, 205111 (2020).
- [45] Y. Huang, P. Hosur, and H. K. Pal, Phys. Rev. B **102**, 155429 (2020).
- [46] F. Xie, A. Cowsik, Z.-D. Song, B. Lian, B. A. Bernevig, and N. Regnault, Phys. Rev. B **103**, 205416 (2021).
- [47] M. Ochi, M. Koshino, and K. Kuroki, Phys. Rev. B **98**, 081102 (2018).
- [48] J. F. Dodaro, S. A. Kivelson, Y. Schattner, X. Q. Sun, and C. Wang, Phys. Rev. B **98**, 075154 (2018).
- [49] P. Potasz, M. Xie, and A. H. MacDonald, arXiv e-prints, arXiv:2102.02256 (2021), arXiv:2102.02256 [cond-mat.str-el].
- [50] O. Vafeek and J. Kang, Phys. Rev. Lett. **125**, 257602 (2020).
- [51] J. Kang and O. Vafeek, Phys. Rev. Lett. **122**, 246401 (2019).
- [52] Z.-D. Song, B. Lian, N. Regnault, and B. A. Bernevig, Phys. Rev. B **103**, 205412 (2021).
- [53] B. A. Bernevig, Z.-D. Song, N. Regnault, and B. Lian, Phys. Rev. B **103**, 205413 (2021).
- [54] B. Lian, Z.-D. Song, N. Regnault, D. K. Efetov, A. Yazdani, and B. A. Bernevig, Phys. Rev. B **103**, 205414 (2021).
- [55] B. A. Bernevig, B. Lian, A. Cowsik, F. Xie, N. Regnault, and Z.-D. Song, Phys. Rev. B **103**, 205415 (2021).
- [56] Y. Alavirad and J. Sau, Phys. Rev. B **102**, 235123 (2020).
- [57] J. E. Hirsch, Phys. Rev. B **31**, 4403 (1985).
- [58] X. Y. Xu, K. Sun, Y. Schattner, E. Berg, and Z. Y. Meng, Phys. Rev. X **7**, 031058 (2017).
- [59] Z. H. Liu, G. Pan, X. Y. Xu, K. Sun, and Z. Y. Meng, Proceedings of the National Academy of Sciences **116**, 16760 (2019).
- [60] Y. Da Liao, Z. Y. Meng, and X. Y. Xu, Phys. Rev. Lett. **123**, 157601 (2019).
- [61] Y. Da Liao, J. Kang, C. N. Breiør, X. Y. Xu, H.-Q. Wu, B. M. Andersen, R. M. Fernandes, and Z. Y. Meng, Phys. Rev. X **11**, 011014 (2021).
- [62] Y.-D. Liao, X.-Y. Xu, Z.-Y. Meng, and J. Kang, Chinese Physics B **30**, 017305 (2021).
- [63] X. Y. Xu, K. T. Law, and P. A. Lee, Phys. Rev. B **98**, 121406 (2018).
- [64] T. Huang, L. Zhang, and T. Ma, Science Bulletin **64**, 310 (2019).
- [65] Z. H. Liu, X. Y. Xu, Y. Qi, K. Sun, and Z. Y. Meng, Phys. Rev. B **99**, 085114 (2019).
- [66] Z. Wang, M. P. Zaletel, R. S. K. Mong, and F. F. Assaad, Phys. Rev. Lett. **126**, 045701 (2021).
- [67] M. Ippoliti, R. S. K. Mong, F. F. Assaad, and M. P. Zaletel, Phys. Rev. B **98**, 235108 (2018).
- [68] The symmetry properties of the form factor and the proofs of the sign structure of the fermion determinant, the QMC measurements and brief description of the stochastic analytic continuation, are presented in this Supplemental Material.
- [69] F. Assaad and H. Evertz, “World-line and determinantal quantum monte carlo methods for spins, phonons and electrons,” in *Computational Many-Particle Physics*, edited by H. Fehske, R. Schneider, and A. Weiße (Springer Berlin Heidelberg, Berlin, Heidelberg, 2008) pp. 277–356.
- [70] X. Y. Xu, Z. H. Liu, G. Pan, Y. Qi, K. Sun, and Z. Y. Meng, Journal of Physics: Condensed Matter **31**, 463001 (2019).
- [71] J. Y. Lee, J. Hofmann, E. Khalaf, A. Vishwanath, and E. Berg, APS March Meeting **S43**, 00013 (2021).
- [72] J. S. Hofmann, E. Khalaf, A. Vishwanath, E. Berg, and J. Y. Lee, arXiv e-prints, arXiv:2105.12112 (2021), arXiv:2105.12112 [cond-mat.str-el].
- [73] A. W. Sandvik, Phys. Rev. B **57**, 10287 (1998).
- [74] K. Beach, arXiv preprint cond-mat/0403055 (2004).
- [75] A. W. Sandvik, Phys. Rev. E **94**, 063308 (2016).
- [76] O. F. Syljuåsen, Phys. Rev. B **78**, 174429 (2008).
- [77] H. Shao, Y. Q. Qin, S. Capponi, S. Chesi, Z. Y. Meng, and A. W. Sandvik, Phys. Rev. X **7**, 041072 (2017).
- [78] G.-Y. Sun, Y.-C. Wang, C. Fang, Y. Qi, M. Cheng, and Z. Y. Meng, Phys. Rev. Lett. **121**, 077201 (2018).
- [79] N. Ma, G.-Y. Sun, Y.-Z. You, C. Xu, A. Vishwanath, A. W. Sandvik, and Z. Y. Meng, Phys. Rev. B **98**, 174421 (2018).
- [80] C.-J. Huang, Y. Deng, Y. Wan, and Z. Y. Meng, Phys. Rev. Lett. **120**, 167202 (2018).
- [81] Z. Yan, Y.-C. Wang, N. Ma, Y. Qi, and Z. Y. Meng, npj Quantum Materials **6**, 1 (2021).
- [82] H. Li, Y. Da Liao, B.-B. Chen, X.-T. Zeng, X.-L. Sheng, Y. Qi, Z. Y. Meng, and W. Li, Nature communications **11**, 1 (2020).

- [83] Z. Hu, Z. Ma, Y.-D. Liao, H. Li, C. Ma, Y. Cui, Y. Shang-guan, Z. Huang, Y. Qi, W. Li, *et al.*, Nature communications **11**, 1 (2020).
- [84] C. Zhou, Z. Yan, H.-Q. Wu, K. Sun, O. A. Starykh, and Z. Y. Meng, arXiv preprint arXiv:2007.12715 (2020).
- [85] Y.-C. Wang, Z. Yan, C. Wang, Y. Qi, and Z. Y. Meng, Phys. Rev. B **103**, 014408 (2021).
- [86] W. Jiang, Y. Liu, A. Klein, Y. Wang, K. Sun, A. V. Chubukov, and Z. Y. Meng, arXiv preprint arXiv:2105.03639 (2021).
- [87] X. Y. Xu, A. Klein, K. Sun, A. V. Chubukov, and Z. Y. Meng, npj Quantum Materials **5**, 65 (2020).
- [88] W. Wang, A. Davis, G. Pan, Y. Wang, and Z. Y. Meng, Phys. Rev. B **103**, 195108 (2021).
- [89] G. Pan, W. Wang, A. Davis, Y. Wang, and Z. Y. Meng, Phys. Rev. Research **3**, 013250 (2021).
- [90] C. Chen, T. Yuan, Y. Qi, and Z. Y. Meng, Phys. Rev. B **103**, 165131 (2021).

Supplemental Material for "Momentum space quantum Monte Carlo on twisted bilayer Graphene"

I. PROPERTIES OF THE FORM FACTOR λ AND PROOF OF THE SIGN STRUCTURE

Here we follow the discussion in band basis as in Ref.[53].

The Hermiticity condition for λ is

$$\lambda_{m,n,\tau}(\mathbf{k}, \mathbf{k} + \mathbf{q} + \mathbf{G}) = \lambda_{n,m,\tau}^*(\mathbf{k} + \mathbf{q} + \mathbf{G}, \mathbf{k}). \quad (5)$$

The $C_{2z}T$ symmetry operates on λ as

$$\lambda_{m,n,\tau}(\mathbf{k}, \mathbf{k} + \mathbf{q} + \mathbf{G}) = \lambda_{m,n,\tau}^*(\mathbf{k}, \mathbf{k} + \mathbf{q} + \mathbf{G}), \quad (6)$$

which means λ is real.

The $C_{2z}P$ symmetry operates on λ as

$$\lambda_{m,n,\tau}(\mathbf{k}, \mathbf{k} + \mathbf{q} + \mathbf{G}) = m * n * \lambda_{-m,-n,-\tau}(\mathbf{k}, \mathbf{k} + \mathbf{q} + \mathbf{G}). \quad (7)$$

Based on these relations, we can derive the Statement 3 in the main text as:

$$\begin{aligned} \delta\rho_{\mathbf{q}+\mathbf{G},-\tau} &= \sum_{\mathbf{k},m,n} \lambda_{m,n,-\tau}(\mathbf{k}, \mathbf{k} + \mathbf{q} + \mathbf{G}) (d_{\mathbf{k},m,-\tau}^\dagger d_{\mathbf{k}+\mathbf{q},n,-\tau} - \frac{1}{2}\delta_{\mathbf{q},0}\delta_{m,n}) \\ &= \sum_{\mathbf{k},m,n} -m * n * \lambda_{m,n,\tau}(\mathbf{k}, \mathbf{k} + \mathbf{q} + \mathbf{G}) (d_{\mathbf{k}+\mathbf{q},-n,-\tau} d_{\mathbf{k},-m,-\tau}^\dagger - \frac{1}{2}\delta_{\mathbf{q},0}\delta_{m,n}) \\ &= \sum_{\mathbf{k},m,n} -\lambda_{m,n,\tau}(\mathbf{k}, \mathbf{k} + \mathbf{q} + \mathbf{G}) (\tilde{d}_{\mathbf{k}+\mathbf{q},n,-\tau}^\dagger \tilde{d}_{\mathbf{k},m,-\tau} - \frac{1}{2}\delta_{\mathbf{q},0}\delta_{m,n}) \\ &= \sum_{\mathbf{k},m,n} -\lambda_{n,m,\tau}(\mathbf{k}, \mathbf{k} - \mathbf{q} - \mathbf{G}) (\tilde{d}_{\mathbf{k},n,-\tau}^\dagger \tilde{d}_{\mathbf{k}-\mathbf{q},m,-\tau} - \frac{1}{2}\delta_{\mathbf{q},0}\delta_{m,n}) \end{aligned} \quad (8)$$

Here $\tilde{d}_{\mathbf{k},m,-\tau} = m * d_{\mathbf{k},-m,-\tau}^\dagger$, $m, n \in \{\pm 1\}$. According to the last line, single-particle matrices in the fermion determinant between two valleys satisfy $\delta\rho_{\mathbf{q}+\mathbf{G},-\tau} = -\delta\rho_{-\mathbf{q}-\mathbf{G},\tau}$. Besides, this transformation does not change kinetic terms. Since

$$\varepsilon_{m,\tau}(\mathbf{k}) = -\varepsilon_{-m,\tau}(-\mathbf{k}) = \varepsilon_{m,-\tau}(-\mathbf{k}) \quad (9)$$

So that

$$\begin{aligned} &\varepsilon_{m,\tau}(\mathbf{k}) d_{\mathbf{k},m,\tau}^\dagger d_{\mathbf{k},m,\tau} + \varepsilon_{-m,\tau}(-\mathbf{k}) d_{-\mathbf{k},-m,\tau}^\dagger d_{-\mathbf{k},-m,\tau} \\ &= \varepsilon_{m,\tau}(\mathbf{k}) (d_{\mathbf{k},m,\tau}^\dagger d_{\mathbf{k},m,\tau} - d_{-\mathbf{k},-m,\tau}^\dagger d_{-\mathbf{k},-m,\tau}) \end{aligned} \quad (10)$$

$$\begin{aligned} &\varepsilon_{-m,-\tau}(\mathbf{k}) d_{\mathbf{k},-m,-\tau}^\dagger d_{\mathbf{k},-m,-\tau} + \varepsilon_{m,-\tau}(-\mathbf{k}) d_{-\mathbf{k},m,-\tau}^\dagger d_{-\mathbf{k},m,-\tau} \\ &= \varepsilon_{m,\tau}(\mathbf{k}) (d_{\mathbf{k},-m,-\tau}^\dagger d_{\mathbf{k},-m,-\tau} - d_{-\mathbf{k},m,-\tau}^\dagger d_{-\mathbf{k},m,-\tau}) \\ &= \varepsilon_{m,\tau}(\mathbf{k}) (\tilde{d}_{\mathbf{k},m,-\tau}^\dagger \tilde{d}_{\mathbf{k},m,-\tau} - \tilde{d}_{-\mathbf{k},-m,-\tau}^\dagger \tilde{d}_{-\mathbf{k},-m,-\tau}) \end{aligned} \quad (11)$$

One can see kinetic terms can be viewed as complex conjugated between two valleys since the dispersion $\varepsilon_{m,\tau}(\mathbf{k})$ is real. We note similar observation, that the TBG Hamiltonian at CNP after QMC decoupling is invariant under anti-unitary particle-hole symmetry, is also pointed out in Refs. [71, 72].

We derive the Statement 2 in another way, different from that in the main text, and then discuss the flat band kinetic terms in this case.

$$\begin{aligned} \delta\rho_{\mathbf{q}+\mathbf{G},-s} &= \sum_{\mathbf{k},m,n} \lambda_{m,n}(\mathbf{k}, \mathbf{k} + \mathbf{q} + \mathbf{G}) (d_{\mathbf{k},m,-s}^\dagger d_{\mathbf{k}+\mathbf{q},n,-s} - \frac{1}{2}\delta_{\mathbf{q},0}\delta_{m,n}) \\ &= \sum_{\mathbf{k},m,n} -\lambda_{n,m}(\mathbf{k}, \mathbf{k} - \mathbf{q} - \mathbf{G}) (d_{\mathbf{k},n,-s} d_{\mathbf{k}-\mathbf{q},m,-s}^\dagger - \frac{1}{2}\delta_{\mathbf{q},0}\delta_{m,n}) \\ &= \sum_{\mathbf{k},m,n} -\lambda_{n,m}(\mathbf{k}, \mathbf{k} - \mathbf{q} - \mathbf{G}) (\tilde{d}_{\mathbf{k},n,-s}^\dagger \tilde{d}_{\mathbf{k}-\mathbf{q},m,-s} - \frac{1}{2}\delta_{\mathbf{q},0}\delta_{m,n}) \end{aligned} \quad (12)$$

In the last line we just define $\tilde{d}_{\mathbf{k},m,-s} = d_{\mathbf{k},m,-s}^\dagger$, single-particle matrices in the fermion determinant between two spins also satisfy $\delta\rho_{\mathbf{q}+\mathbf{G},-s} = -\delta\rho_{-\mathbf{q}-\mathbf{G},s}$. But this transformation add a minus sign to the kinetic terms.

$$\begin{aligned} & \varepsilon_m(\mathbf{k})d_{\mathbf{k},m,-s}^\dagger d_{\mathbf{k},m,-s} + \varepsilon_{-m}(-\mathbf{k})d_{-\mathbf{k},-m,-s}^\dagger d_{-\mathbf{k},-m,-s} \\ &= -\varepsilon_m(\mathbf{k})(d_{\mathbf{k},m,-s}d_{\mathbf{k},m,-s}^\dagger - d_{-\mathbf{k},-m,-s}d_{-\mathbf{k},-m,-s}^\dagger) \\ &= -\varepsilon_m(\mathbf{k})(\tilde{d}_{\mathbf{k},m,-s}^\dagger \tilde{d}_{\mathbf{k},m,-s} - \tilde{d}_{-\mathbf{k},-m,-s}^\dagger \tilde{d}_{-\mathbf{k},-m,-s}) \end{aligned} \quad (13)$$

It is thus not obvious when consider both spin degree of freedom for a single valley, when including the kinetic energy, the QMC simulation is still absent of sign-problem.

II. MEASUREMENT OF THE GREEN'S FUNCTION IN QMC

Here we introduce the measurement of Green's functions in QMC. Generally, average of any observables \hat{O} can be written as,

$$\langle \hat{O} \rangle = \frac{\text{Tr}(\hat{O}e^{-\beta H})}{\text{Tr}(e^{-\beta H})} = \sum_{\{l_{|\mathbf{q}|,t}\}} \frac{P(\{l_{|\mathbf{q}|,t}\}) \text{Tr}[\prod_t \hat{B}_t(\{l_{|\mathbf{q}|,t}\})] \frac{\text{Tr}[\hat{O} \prod_t \hat{B}_t(\{l_{|\mathbf{q}|,t}\})]}{\text{Tr}[\prod_t \hat{B}_t(\{l_{|\mathbf{q}|,t}\})]}}{\sum_{\{l_{|\mathbf{q}|,t}\}} P(\{l_{|\mathbf{q}|,t}\}) \text{Tr}[\prod_t \hat{B}_t(\{l_{|\mathbf{q}|,t}\})]} \quad (14)$$

According to Eq. (4) in the main text, $P(\{l_{|\mathbf{q}|,t}\}) = \prod_t [\prod_{|\mathbf{q}+\mathbf{G}| \neq 0} \frac{1}{16} \gamma(l_{|\mathbf{q}|,t}) \gamma(l_{|\mathbf{q}|,t+\mathbf{G}})]$ and

$$\hat{B}_t(\{l_{|\mathbf{q}|,t}\}) = \prod_{|\mathbf{q}+\mathbf{G}| \neq 0} e^{i\eta(l_{|\mathbf{q}|,t})A_{\mathbf{q}}(\delta\rho_{-\mathbf{q}}+\delta\rho_{\mathbf{q}})} e^{\eta(l_{|\mathbf{q}|,t+\mathbf{G}})A_{\mathbf{q}}(\delta\rho_{-\mathbf{q}}-\delta\rho_{\mathbf{q}})}, \quad (15)$$

respectively.

Since M_j is now of the form of fermion bilinear, one can trace out the fermion operator to obtain the determinant

$$\text{Tr}[e^{M_1}e^{M_2}...e^{M_n}] = \det[I + e^{M_1}e^{M_2}...e^{M_n}], \quad (16)$$

the obtained determinant is the single particle fermion determinant for QMC. Exact constant terms in $\hat{B}(\{l_{|\mathbf{q}|,t}\})$ as $e^{-\frac{1}{2}\sum_j \text{Tr}(M_j)}$ represent the left part in the single particle basis e^{M_t} , and it is from such structure

$$e^{-\frac{1}{2}\sum_j \text{Tr}(M_j)} \det(I + e^{M_1}e^{M_2}...e^{M_n}) \quad (17)$$

we prove the Statement 1 in the main text.

Now consider operator $\hat{O} = d_i(\tau)d_j^\dagger(\tau)$, which is the single-particle Green's function $G(\tau,\tau)_{i,j} = \langle d_i(\tau)d_j^\dagger(\tau) \rangle$ in QMC,

$$\frac{\text{Tr}[\prod_{t_1 > \tau} \hat{B}_{t_1}(\{l_{|\mathbf{q}|,t}\}) d_i(\tau) d_j^\dagger(\tau) \prod_{t_2 \leq \tau} \hat{B}_{t_2}(\{l_{|\mathbf{q}|,t}\})]}{\text{Tr}[\prod_t \hat{B}_t(\{l_{|\mathbf{q}|,t}\})]} = (I + e^{M_\tau} e^{M_{\tau-1}} ... e^{M_1} \cdot e^{M_n} e^{M_{n-1}} ... e^{M_{\tau+1}})^{-1}_{i,j}. \quad (18)$$

Statement 4 If there is no kinetic term, Green's function $G(\tau,\tau)_{i,j}$ should always be diagonal with all non-zero elements 0.5.

Proof For a certain configuration $U_S = B_{1,s_1}B_{2,s_2}...B_{n,s_n}$, ignoring matrix commutation in each B_{t,s_1} , we can always find another configuration $U_{S'} = B_{1,-s_n}...B_{n-1,-s_2}B_{n,-s_1} = U_S^{-1}$ with the same weight

$$e^{-\frac{1}{2}\sum_j \text{Tr}(M_j)} \det(I + e^{M_1}e^{M_2}...e^{M_n}) = e^{\frac{1}{2}\sum_j \text{Tr}(M_j)} \det(I + (e^{M_1}e^{M_2}...e^{M_n})^{-1}). \quad (19)$$

We add Green's function $G(\tau,\tau)_{i,j}$ of this pair configurations together, which is $(I + e^{M_1}e^{M_2}...e^{M_n})^{-1} + (I + (e^{M_1}e^{M_2}...e^{M_n})^{-1})^{-1} = I$. Remember we need to divide it by 2 for average of these two configurations, therefore after sampling and average, $G(\tau,\tau)_{i,j}$ should always be diagonal with all non-zero elements 0.5.

Besides, consider $G(\tau,0)_{i,j} = \langle d_i(\tau)d_j^\dagger(0) \rangle$,

$$\frac{\text{Tr}[\prod_{t_1 > \tau} \hat{B}_{t_1}(\{l_{|\mathbf{q}|,t}\}) d_i(\tau) \prod_{t_2 \leq \tau} \hat{B}_{t_2}(\{l_{|\mathbf{q}|,t}\}) d_j^\dagger(0)]}{\text{Tr}[\prod_t \hat{B}_t(\{l_{|\mathbf{q}|,t}\})]} = (G(\tau,\tau) \cdot e^{M_\tau} e^{M_{\tau-1}} ... e^{M_1})_{i,j} \quad (20)$$

We also introduce a useful way below to obtain real valued measurables for other fillings, in which, the sign of the weight is always real. The definition of $\delta\rho_{\mathbf{q}+\mathbf{G}}$ should be rewritten as:

$$\delta\rho_{\mathbf{q}+\mathbf{G}} = \sum_{\mathbf{k} \in mBZ, m_1, m_2, \tau, s} \lambda_{m_1, m_2, \tau}(\mathbf{k}, \mathbf{k} + \mathbf{q} + \mathbf{G}) (d_{\mathbf{k}, m_1, \tau, s}^\dagger d_{\mathbf{k}+\mathbf{q}, m_2, \tau, s} - C \delta_{\mathbf{q}, 0} \delta_{m_1, m_2}) = (\delta\rho_{-\mathbf{q}-\mathbf{G}})^\dagger. \quad (21)$$

Here C can be any real number.

Assume we would like to measure $\langle F \rangle = \langle F^* \rangle = \frac{\langle F + F^* \rangle}{2}$. For any configuration S , we can define a dual configuration $-S$. For $-S$, in $\hat{B}_t(\{l_{|\mathbf{q}|, t}\}) = \prod_{|\mathbf{q}+\mathbf{G}| \neq 0} e^{i\eta(l_{|\mathbf{q}|, t}) A_{\mathbf{q}}(\delta\rho_{-\mathbf{q}} + \delta\rho_{\mathbf{q}})} e^{\eta(l_{|\mathbf{q}|, 2, t}) A_{\mathbf{q}}(\delta\rho_{-\mathbf{q}} - \delta\rho_{\mathbf{q}})}$, all $\eta(l_{|\mathbf{q}|, t})$ do not change and all other $\eta(l_{|\mathbf{q}|, t})$ change to $-\eta(l_{|\mathbf{q}|, t})$. Then one can see $\hat{B}_t(\{l_{|\mathbf{q}|, t}\})$ change to $\hat{B}_t^*(\{l_{|\mathbf{q}|, t}\})$, weight $P_S = e^{-C \sum_j \text{Tr}(M_j)} \det(I + e^{M_1} e^{M_2} \dots e^{M_n})$ changes to $P_{-S} = \left[e^{-C \sum_j \text{Tr}(M_j)} \det(I + e^{M_1} e^{M_2} \dots e^{M_n}) \right]^* = P_S^*$. It is obvious that

$$\frac{\langle F + F^* \rangle}{2} = \sum_{\{S\}} \frac{P_S F_S + P_{-S} F_{-S}^*}{2} = \sum_{\{S\}} \text{Re}(P_S) F_S. \quad (22)$$

We conclude here, to measure real measurables for any filling, one just need to see real part of weight as an effective weight.

III. STOCHASTIC ANALYTIC CONTINUATION (SAC) METHOD

Here we use the stochastic analytic continuation (SAC) method [73–77] to obtain the spectral function $A_{\vec{k}}(\omega)$, where $A_{\vec{k}}(\omega) = -(1/\pi) \text{Im} G_{\vec{k}}^{ret}(\omega)$. The relationship of $A_{\vec{k}}(\omega)$ and correlation function in imaginary time is:

$$G_{\vec{k}}(\tau) = \int_{-\infty}^{\infty} d\omega \left[\frac{e^{-\omega\tau}}{1 + e^{-\beta\omega}} \right] A_{\vec{k}}(\omega) \quad (23)$$

The following quantity χ^2 is used to evaluate the quality of the fit, where we first give an very generic variational ansatz of the spectrum $A(\omega)$ and then carry out the above Laplacian transformation and use the obtained Green's function to compare (fit) with the QMC Green's function and optimize the ansatz according to the χ^2 stochastically:

$$\chi^2 = \sum_{ij} \left(\bar{G}(\tau_i) - \int_{-\infty}^{\infty} d\omega \left[\frac{e^{-\omega\tau_i}}{1 + e^{-\beta\omega}} \right] A(\omega) \right) (C^{-1})_{ij} \left(\bar{G}(\tau_j) - \int_{-\infty}^{\infty} d\omega \left[\frac{e^{-\omega\tau_j}}{1 + e^{-\beta\omega}} \right] A(\omega) \right) \quad (24)$$

where

$$C_{ij} = \frac{1}{N_b(N_b - 1)} \sum_{b=1}^{N_b} (G^b(\tau_i) - \bar{G}(\tau_i)) (G^b(\tau_j) - \bar{G}(\tau_j)) \quad (25)$$

Here $\bar{G}(\tau_i)$ is the Monte Carlo average of Green's functions of N_b bins.

In order to obtain the optimized spectral function, we perform the Monte Carlo sampling [75, 76] to improve it with the QMC Green's function. The ansatz of the spectral function is $A(\omega) = \sum_{i=1}^{N_\omega} A_i \delta(\omega - \omega_i)$ and the weight of such Monte Carlo configuration is:

$$W \sim \exp\left(-\frac{\chi^2}{2\Theta_T}\right) \quad (26)$$

Here Θ_T is an analogy to temperature. We carry out simulated annealing method and at different Θ_T we compute the average $\langle \chi^2 \rangle$, finally choose the converged Θ_T to satisfy:

$$\langle \chi^2 \rangle = \chi_{\min}^2 + a\sqrt{\chi_{\min}^2} \quad (27)$$

usually we set $a = 2$, and it is from such optimized Θ and χ^2 , we further compute the ensemble average of the spectra as the final ones to present in the main text.